Nondivergent Planetary Oscillations in Midlatitude Ocean Basins with Continental Shelves

ARTHUR J. MILLER

Scripps Institution of Oceanography, La Jolla, CA 92093

(Manuscript received 27 December 1985, in final form 28 May 1986)

ABSTRACT

Free oscillations in square, midlatitude basins with continental shelves and planetary vorticity gradients are numerically computed using the nondivergent shallow-water equations. The topography may rend a planetary mode into a family of basinwide modes, each comparable to the flat-bottom counterpart in frequency and midbasin structure. This phenomenon can be interpreted in terms of coupled planetary wave–shelf wave oscillations. The mechanism provides an alternative to strong dissipation in explaining broadbanded planetary-wave signals observed in tide gauge records.

1. Introduction

Barotropic free oscillations of ocean basins on a rotating earth have been theoretically predicted (e.g., Lamb, 1932, Ch. 8) for a variety of simplified geometries. For example, Longuet-Higgins and Pond (1970) considered a hemispherical basin of constant depth as a model of the Pacific Ocean and discussed solutions in terms of gravity, planetary and other new types of wave motion.

More recently, Platzman and collaborators (1978; 1981b; 1985) have developed a model world ocean with topography and numerically calculated barotropic normal modes of period between 8 and 96 hours. Gravity provided the dominant restoring force for modes with period less than about 30 hours. Longer period oscillations were vorticity waves predominantly trapped to strong topographic features, sometimes coexistent with very weak planetary wavelike flow. Platzman's finding of no modes significantly controlled by the planetary vorticity gradient was surprising, although perhaps adumbrated by previous studies of the strong effects of topography on vorticity waves (e.g., Rhines and Bretherton, 1973; Anderson and Killworth, 1977). It should be noted that the topography in Platzman's model may not have been sufficiently resolved to model these vorticity modes accurately.

Sea level records from island tide gauge stations provide the best possibility for observing basin-scale oscillations excited at resonance. Definitive observations of either gravity or vorticity modes, as evidenced by resonant peaks in power spectra, are still lacking (see Luther, 1983, for historical background); however, Luther (1980; 1982) presents inter-island coherence spectra that suggest the presence of a basinwide, Pacific Ocean, planetary mode having a period of about 5 days. The response is directly observable only as a broadband peak (or shoulder) in sea-level power spectra. Consequently, Luther's estimate of $Q \approx 4$,[1] on the assumption of a single resonant mode, implies quite large frictional damping. A direct estimate, such as this of dissipation for large-scale flow, bears strongly on oceanic modeling assumptions.

In the light of Platzman's computations and the many theoretical studies of the strong effect of topographic vortex stretching on vorticity waves, Luther's observations seem puzzling. Are there analogues of flat-bottom, barotropic, planetary oscillations in oceanic basins? Is it strong dissipation or planetary mode spectral density that produces the aforementioned broadband response? These questions have motivated numerical investigations of the effects of topography on Rossby modes using the eigencodes of Platzman (1978). We have adapted these codes to solve nondivergent approximations of the shallow-water equations with high resolution over variable relief in a square basin.

We find that a particularly intriguing phenomenon occurs when a continental shelf surrounds an otherwise flat basin. A given, nondegenerate (singlet), flat-bottom Rossby mode may be rent into a family of basinwide modes, each member of which resembles the flat-bottom counterpart in frequency and midocean structure. This effect appears best interpreted in terms of coupled planetary wave–shelf wave oscillations. We emphasize that the effect of the shelf is a strong perturbation of

[1] The resonance quality Q is defined to be $f/\Delta f_{1/2}$, where f is the free mode frequency and $\Delta f_{1/2}$ is the resonant peak bandwidth at the one-half power point of the freely decaying mode spectrum (see Luther, 1982).

the spectrum. Thus, this phenomenon is distinct from, say, the splitting of degenerate (multiplet) normal modes of the solid earth by weak perturbations (e.g., Dahlen, 1968). With moderate dissipation, the present effect could cause peak-width Qs of resonant planetary modes as estimated from tide gauge data to be unrealistically small.

Model resolution here is limited to 50 km in a 4000 km square basin, so that the idealized shelf is far from realistic. The importance of baroclinicity must also be investigated since internal oscillations can possess fast time scales near steep topography and in low latitudes. However, our intuitive model of coupled oscillations (section 4) may provide insight for the dynamics when steeper shelves or internal oscillations are present. The model also may be able to estimate time scales of leakage of planetary wave energy onto and off continental shelves.

The following section describes two nondivergent models for vorticity modes. Section 3 presents numerical eigensolutions for these equations. A simplified model of the response is put forth in section 4. Discussion of the results and conclusions are contained in sections 5 and 6, respectively.

2. Rigid-lid models of vorticity modes

Consider a closed, midlatitude, homogeneous (or strongly stratified, as in Miles, 1974) ocean in a basin of nonuniform depth. In Cartesian geometry, free oscillations satisfy the linearized, unforced, inviscid shallow-water equations (Gill, 1982, §9.9)

$$u_t - fv = -g\eta_x \tag{2.1a}$$

$$v_t + fu = -g\eta_y \tag{2.1b}$$

$$\eta_t + (Hu)_x + (Hv)_y = 0 \tag{2.1c}$$

with zero normal velocity on the boundaries. Here u, v, η are eastward velocity, northward velocity and surface elevation, g is constant gravitational acceleration, $f(y)$ the Coriolis frequency, and $H(x, y)$ the fluid depth. The difficulty in solving these equations and others derived from them lies in their nonseparability and their nonconstant coefficients. For these reasons, numerical methods are needed to obtain solutions for realistic bathymetry.

We are here interested only in the low-frequency, vorticity wave solutions of (2.1). In order to filter the high-frequency gravity waves and, perforce, the Kelvin waves, we employ (two) rigid-lid analogues of (2.1). An additional benefit of the rigidlid is to simplify the model boundary condition. The primary effect of the rigid-lid approximation is to modify the phase speeds of waves longer than the deformation radius $\equiv (gH)^{1/2}f^{-1}$. Flierl (1977) extensively discusses this effect for flat-bottom situations.

Perhaps the simplest and most familiar approximation for vorticity waves in this system is quasi-geostrophy (Pedlosky, 1979). Inherent assumptions are that frequencies are much less than f, depth deviations, $h = H_0 - H$, are linearized about a representative depth H_0 and horizontal length scales of flow are small compared with the radius of the earth. With the rigid-lid assumption, these imply that (2.1) reduces to

$$\nabla^2\psi_t + \beta\psi_x + \frac{f_0}{H_0}J(\psi, h) = 0, \tag{2.2}$$

hereafter designated as the rigid-lid, *quasi-geostrophic equation*. The velocity streamfunction, ψ, is defined by

$$-\psi_y = u, \quad \psi_x = v, \tag{2.3a,b}$$

the β-plane approximation, $f \equiv f_0$ and $df/dy \equiv \beta$ (both constant), is invoked, and the Jacobian $J(A, B) \equiv -A_yB_x + A_xB_y$. Let $\psi = \mathrm{Re}[e^{i\sigma_n t}\phi_n(x, y)]$ so that, with $\phi_n = 0$ on the boundary,

$$i\sigma_n\nabla^2\phi_n + J\left(\phi_n, \beta y + \frac{f_0 h}{H_0}\right) = 0 \tag{2.4}$$

forms a self-adjoint generalized eigenproblem in the frequency, σ_n (eigenvalue), and streamfunction, ϕ_n (eigenfunction).

More generally, we can incorporate strong depth deviations and spatially variable Coriolis effects by applying the rigid-lid assumption directly to (2.1c) so that

$$\nabla \cdot (H\mathbf{u}) = 0, \tag{2.5}$$

and we can define a volume transport streamfunction

$$-\Psi_y = uH, \quad \Psi_x = vH. \tag{2.6a,b}$$

Taking the curl of (2.1a,b) and using (2.5), we have

$$\nabla \cdot \left(\frac{\nabla\Psi_t}{H}\right) + J\left(\Psi, \frac{f}{H}\right) = 0, \tag{2.7}$$

hereafter designated as the *volume-transport equation*. Let $\Psi = \mathrm{Re}[e^{i\sigma_n t}\Phi_n(x, y)]$ so that

$$i\sigma_n\nabla \cdot \left(\frac{\nabla\Phi_n}{H}\right) + J\left(\Phi_n, \frac{f}{H}\right) = 0 \tag{2.8}$$

with $\Phi_n = 0$ on the boundary forms the eigenproblem analogous to (2.4).

Discrete versions of both (2.4) and (2.8) form matrix eigenproblems of the form

$$i\mathbf{A}\mathbf{Z}_n = \sigma_n\mathbf{B}\mathbf{Z}_n, \tag{2.9}$$

where $\mathbf{A}$ is a real, skew-symmetric, matrix operator, $\mathbf{B}$ is a real, symmetric, matrix operator and $\mathbf{Z}_n$ is the discrete vector analogue of the streamfunction. The general form of (2.9) is analogous to Platzman's (1978) finite element model. Thus, (2.4) and (2.8) may be solved using appropriate adaptations of Platzman's (1978; 1981a) eigencodes (see Miller, 1986, for details). The Jacobian is discretized according to Arakawa's (1966) formalism, while the gradient operators are discretized with standard centered differences. Core stor-

age on the Cray-1 at NCAR limits us to 50 km resolution of the streamfunction in a 4000 km square basin. This results in a 6241 square eigenproblem. Eigensolutions of (2.9) yield normalized residuals which are typically less than 10^{-8}. Normalized error bounds (see Platzman, 1981a,b) for the eigenvalues and eigenfunctions are then typically less than 10^{-12} and 10^{-6}, respectively. The numerical procedure is further discussed in section 3.

To model a continental shelf, we employ the Gaussian shelf depicted in Fig. 1a, b and described by

$$H = H_0 - D \exp\left[-\frac{(\xi - \xi_0)^2}{L^2}\right], \qquad (2.10)$$

where ξ_0 is a boundary point, ξ the coordinate normal to the boundary, $L = 250$ km is the characteristic width of the shelf, $H_0 = 5000$ m is the interior ocean depth and $H_0 - D$ is the shelf depth at the boundary. The choice of L is limited by the grid resolution. In the corners of the basin the topography is smoothed by choosing the shallowest depths of the overlapping shelves.

3. Numerical eigensolutions

In this section we present numerical solutions of (2.4) and (2.8). Platzman's (1978) world ocean, normal modes code has been adapted to solve the problem at hand. (Christensen's, 1973, perturbative technique for solving a similar shelved basin problem is inappropriate for generating a full spectral band of solutions.) Solutions of both (2.4) and (2.8) occur in conjugate pairs corresponding to positive and negative frequency. (Both solutions in a pair give the same real streamfunction.) The Fortran code implements a Lanczos tridiagonalization of an equivalent, standard matrix eigenproblem, formulated with the squared frequency as the eigenvalue. The spectrum of solutions consistently appears in order of decreasing frequency. Lower frequency solutions are increasingly slow to converge. (Expenditure of computer time increases drastically when attempting to increase the convergence of lower frequency solutions.) Upon reaching a solution that has not converged to the desired degree of accuracy (normalized residual less than 10^{-8}), the procedure is terminated. In a typical calculation, we compute the first 50–200 eigenmodes and consume 5–15 minutes of CPU time on the Cray-1 at NCAR. For further discussion of the numerical procedure see Platzman (1978; 1981a) and Miller (1986).

Calculations are carried out here in a 4000 km-square basin with 50 km resolution for three scenarios: (a) f-plane quasi-geostrophic modes with a shelf, (b) β-plane, quasi-geostrophic modes with a shelf and (c) volume-transport modes with a shelf. Case (a) corresponds to (2.4) with $f = f_0$, $\beta = 0$ and depth deviations, $h = H_0 - H(x, y)$. In case (b), (2.4) again applies but with nonzero β. Case (c) corresponds to (2.8) with $f = f_0 + \beta y$, a fully variable linear function of latitude, and $H = H(x, y)$. The f-plane solutions are useful for interpreting solutions which include the β-effect.

a. f-plane quasi-geostrophy with a shelf

The quasi-geostrophic framework restricts us to small depth deviations, h, relative to H_0. Therefore, as an archetypical case, we consider a 3000 m deep continental shelf (Fig. 1b; (2.10) with $D = 2000$ m) surrounding the 5000 m deep, square basin on an f-plane.

The four-fold rotational symmetry of the basin implies that analytical eigenvalues of the continuous problem are four-fold degenerate. For the discrete problem, we find instead that distinct eigenvalues, closely matched in frequency, appear in groups of four. (Note that the small frequency differences between individual eigenvalues within a group are many orders of magnitude above truncation error.) It is finite-differencing error which removes the degeneracies. This loss of degeneracy arises from the perturbation involved in transforming the continuous operator to the discrete operator. In general, perturbing a matrix with degenerate eigenvalues removes the degeneracy yet preserves some measure of closeness (related to the size of the perturbation) of the perturbed eigenvalues to the orig-

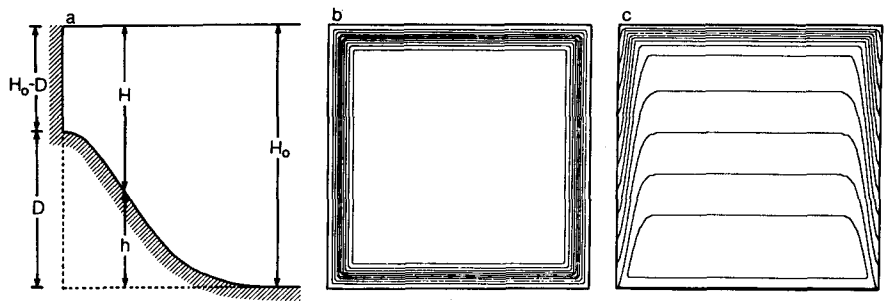

FIG. 1. Basin geometry. (a) Profile of the shelf topography from (2.10). (b) Depth contours h for the case of a 3000 m deep shelf. Here the total depth $H = H_0 - h$ with $H_0 = 5000$ m. (c) f/H contours for the same case. Here $f = f_0 + \beta y$ with $f_0 = 9.3 \times 10^{-5}$ s^{-1} and $\beta = 2.0 \times 10^{-11}$ m^{-1} s^{-1}.

inal degenerate ones (Bunch, private communication, 1986). This interpretation is substantiated by an analogous coarse resolution (100 km) case which yielded larger frequency differences between the nearly degenerate eigenvalues.

The associated eigenfunctions of each virtually degenerate group are orthogonal to each other and to members of other groups. Basin symmetry manifests itself in the eigenfunctions; when rotated in 90° increments, each eigenfunction remains a solution for the same eigenvalue.

The fundamental shelf wave group (Fig. 2) has one amplitude maximum along and across each shelf, with phases propagating with shallower depth on the right. Lower frequency groups contain more amplitude maxima, shorter wavelength phase variations, and larger frequency spreads within the group (indicative of the increase in discretization error for these smaller scale solutions). The four modes of the fundamental group may be linearly combined to form four new modes, each with an overwhelmingly localized response on one shelf region (northern, southern, western or eastern shelf), and a minute response on the others. Lower frequency groups may be similarly recombined, but they cannot be so highly localized.

The trapping mechanism which localizes response on one shelf region is anticipated from shelf-wave theory. Vorticity waves on a shelf will reflect strongly from the basin wall boundary and the seaward edge of the shelf. The sharp changes in depth contours encountered at shelf intersections will partially reflect and partially transmit incident waves. One can then envision con-

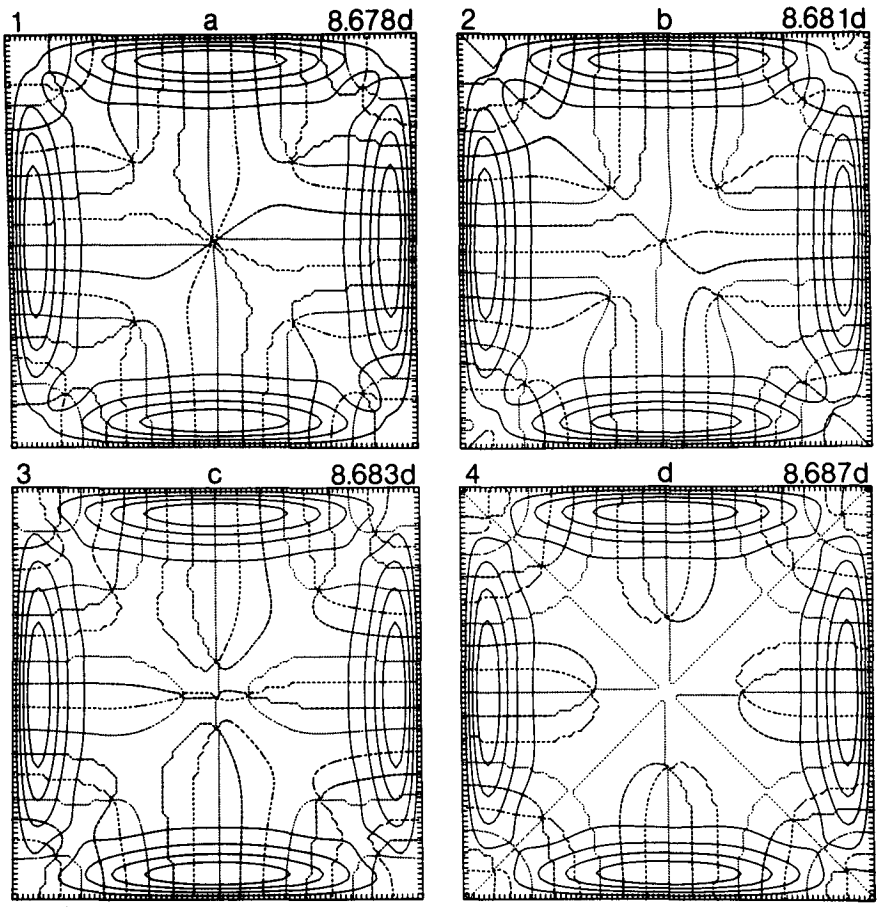

FIG. 2. Quasi-geostrophic f-plane case with a 3000 m shelf depth. The first (highest frequency) four eigenfunctions. Above each plot is (left) the mode number and (right) the mode period in days. The modes are normalized to unit amplitude for contouring. Solid lines are constant amplitude in 0.2 intervals. Dashed lines are constant phase in $\pi/3$ intervals. (a) Mode 1, period 8.678 days. (b) Mode 2, period 8.681 days. (c) Mode 3, period 8.683 days. (d) Mode 4, period 8.687 days. These solutions are degenerate analytically but not numerically. Note that the amplitude structure on any shelf is very similar for each mode. The phases are oriented such that these four modes may be linearly combined to produce four independent modes each of which is overwhelmingly localized on one shelf region. Lower frequency sets of shelf modes (not shown) are less able to be localized.

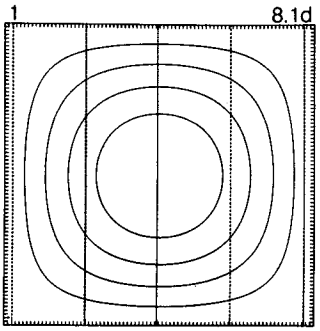

FIG. 3. Quasi-geostrophic β-plane case with a flat bottom. The fundamental mode with period 8.1 days. Contouring as in Fig. 2.

structing the shelf mode from a small number of shelf waves in a manner analogous to the construction of a Rossby mode in a basin (e.g., Pedlosky, 1979, p. 148). The extent to which a group of four modes cannot be combined to localize response on one shelf region provides an indication of the degree to which incident waves are transmitted around the corners. (Note that in the continuous geometry the localized, or nearly localized, response of a linear combination of four orthogonal, but degenerate, modes remains stationary for all time. The discrete case allows the response to evolve slowly, leaking energy onto adjacent shelves over a time interval proportional to the inverse of the frequency spread of the nearly degenerate group.)

b. β-plane quasi-geostrophy with a shelf

With the same 3000 m shelf depth as in case (a), we include in (2.4) a planetary vorticity gradient which will allow Rossby-like oscillations. Without the shelf, the fundamental Rossby mode (Fig. 3; Pedlosky, 1979, p. 147) has a period of 8.1 days. (The frequency obtained numerically for this mode differs by less than 0.1% from the analytical value.) Without β, the fun-

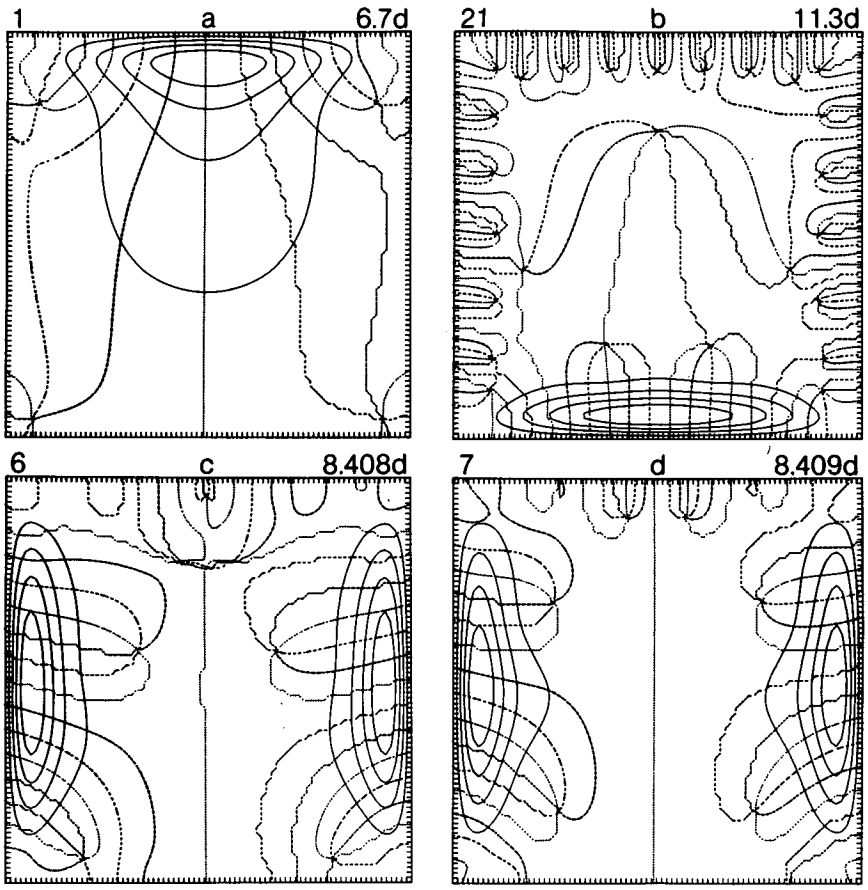

FIG. 4. Quasi-geostrophic β-plane case with a 3000 m shelf depth. Counterparts of the fundamental shelf modes of Fig. 2 when the basin is placed on a β-plane. Contouring as in Fig. 2. (a) Mode 1, period 6.7 days. (b) Mode 21, period 11.3 days. (c) Mode 6, period 8.408 days. (d) Mode 7, period 8.409 days. The β-effect perturbs the virtually degenerate set, causing it to split into two nondegenerate modes and a virtually degenerate pair. Note that mode 1 extends into the interior, suggesting a weak interaction with planetary motion.

damental shelf mode period is 8.7 days (Fig. 2). With the combined effects, the basin supports a fundamental wave period of 6.7 days. This particular wave (Fig. 4a) is strongly localized on the northern shelf where β reinforces the topographic gradient. Thus, the resultant frequency is higher than that due to either effect alone.

The first five modes exhibit a progressively stronger β-like component in the ocean interior, combined with a strong northern shelf response which resembles f-plane shelf-mode structures of section 3a. Modes 4 and 5 (Fig. 5b, c) have interior response very much like the fundamental flat-bottom β-mode. Modes 3 and 10 (Fig. 5a, d) also exhibit an interior response resembling the fundamental β-mode. The appearance of more than one frequency of response for these fundamental β-mode structures is remarkable.

Lower frequency modes are not easily summarized. Some resemble pure shelf waves and some are more aptly described as combination planetary/shelf modes. A strong shelf response may (i) be very localized (e.g., Fig. 4b), (ii) have a decaying "tail" extending into the flat interior (e.g., Fig. 4a), (iii) connect to an interior response which resembles a β-mode (e.g., Figure 5c), or (iv) connect to a more complicated interior response (e.g., Fig. 6). Typically, interior flows interact more strongly with response on the northern shelf than the southern. Evidently, this is due to the sense of the topographic gradient vis-a-vis β; the tendency for phase propagation is westward both in the interior and on the northern shelf while the tendency is eastward on the southern shelf.

The fundamental group of four f-plane shelf modes (Fig. 2) has an interesting fate on the β-plane. The β-effect acts as a standard perturbation which splits the (virtual) quadruplet into two singlets and a doublet. The northern shelf mode appears as the fundamental mode (Fig. 4a) with frequency shifted to a higher value than that of its f-plane analogue (namely, the linear combination of modes from Fig. 2 which localizes response on the northern shelf). The structural change

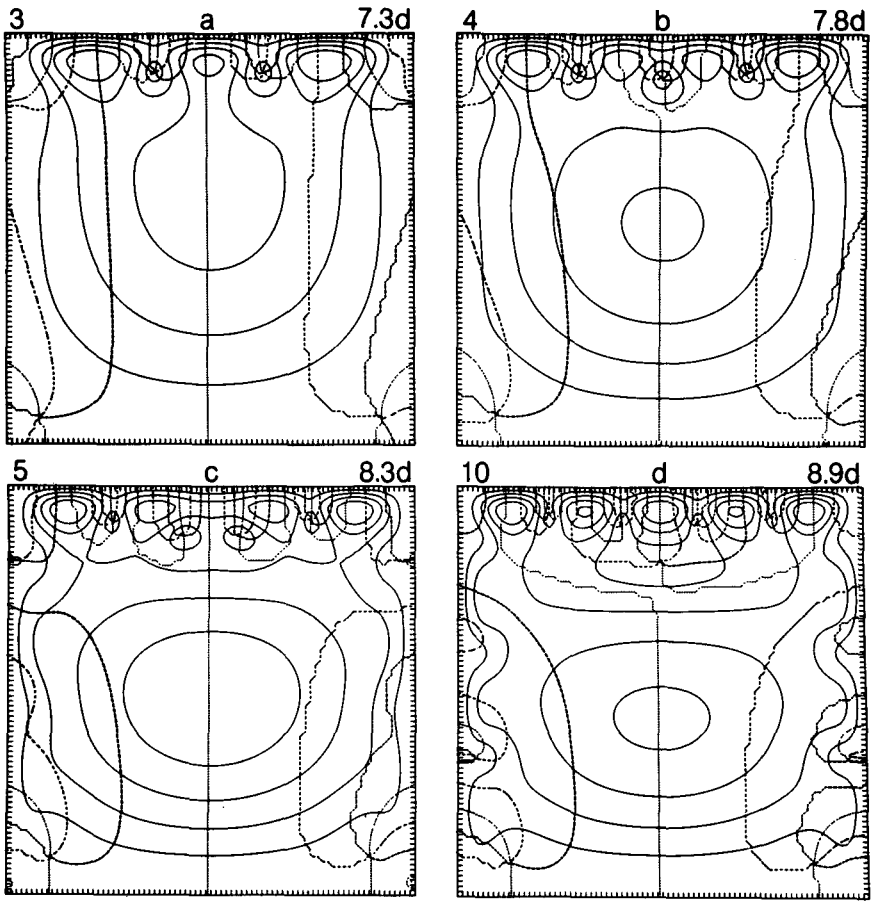

FIG. 5. Quasi-geostrophic β-plane case with a 3000 m shelf depth. Four modes with strong interior response resembling the fundamental flat-bottom β-mode structure of Fig. 3. Contouring as in Fig. 2. (a) Mode 3, period 7.3 days. (b) Mode 4, period 7.8 days. (c) Mode 5, period 8.3 days. (d) Mode 10, period 8.9 days. Note the interaction of the interior response with shelf motion of varying structure.

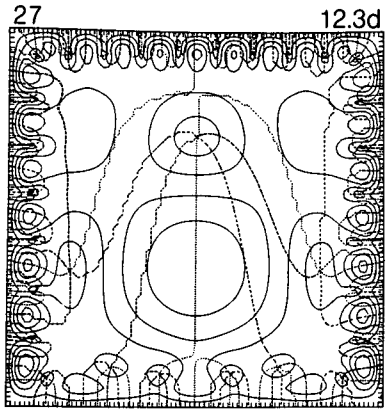

FIG. 6. Quasi-geostrophic β-plane case with a 3000 m shelf depth. An example of a mode with strong interior response which does not particularly correspond to the structure of a single flat-bottom β-mode. Contouring as in Fig. 2. Mode 27, period 12.3 days.

is greatest for this wave, exemplifying the relatively strong interaction between northern shelf waves and interior planetary motion. The southern shelf mode (Fig. 4b) has shifted to a lower frequency due to the (perturbative) β-effect being in opposition to the topographic gradient of the southern shelf. The eastern and western shelf modes remain virtually degenerate (Fig. 4c, d) with frequencies increased slightly over the f-plane situation. Higher groups of shelf modes can behave similarly unless they interact strongly with interior planetary flow or other shelf-mode groups.

c. *Volume-transport flow with a shelf*

Equation (2.8) allows both f and H to be fully variable. For simple comparison with case (b), we employ a linear latitudinal dependence for $f \equiv f_0 + \beta y$ and first discuss the 3000 m shelf depth (contours of f/H are shown in Fig. 1c). The most striking new feature of these solutions is the existence of critical latitudes on the eastern and western shelves (Fig. 7). Northward (southward) of the turning latitudes the response is oscillatory (decaying), suggesting a structural similarity with an Airy function. The topographic strength is modulated by f, which acts as a slowly varying parameter; shelf waves of a particular frequency may exist only northwards of their respective turning latitude (Miller, 1986).

Besides the aforementioned effect, the solutions qualitatively resemble the quasi-geostrophic, β-plane case. Differences between the two cases are primarily due to the stronger effect of topography (i.e., no longer linearized) and the spatial variability of f, which regulates the local topographic strength. The former effect causes shelf-trapped response to have smaller-scale structure compared with quasi-geostrophic response of similar frequency. The latter effect causes shelf waves trapped to the northern (southern) shelf to be of higher (lower) frequency than their quasi-geostrophic counterparts of case (b). Once again, several modes (Fig. 8) have interior response resembling the fundamental, flat-bottom β-mode.

Decreasing the depth of the shelf (2000 and 1000 m depths were employed) yields qualitatively similar results, although we find greater numbers of solutions with interior structure resembling the fundamental β-mode. We also find many modes having strong interior response which bears little resemblance to flat-bottom β-mode structure (as in Fig. 6). It appears that the spectral density of large-scale planetary-like modes is linked to the spectral density of shelf waves with frequency in the β-mode range, the latter increasing with topographic amplitude.

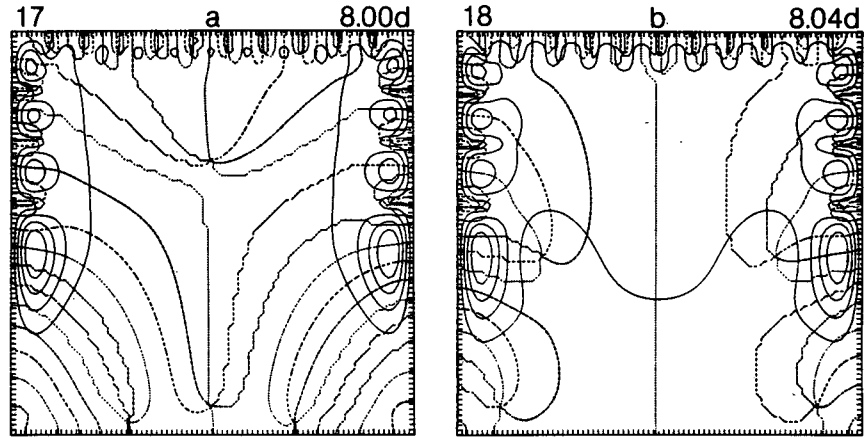

FIG. 7. Volume-transport case with a 3000 m shelf depth. Examples of barotropic shelf waves with turning latitudes. Contouring as in Fig. 2. (a) Mode 17, period 8.00 days. (b) Mode 18, period 8.04 days. The two modes form a virtually degenerate pair as in Fig. 4c, d. The strength of the topographic effect varies due to the spatially variable Coriolis frequency. This results in response structure resembling an Airy function.

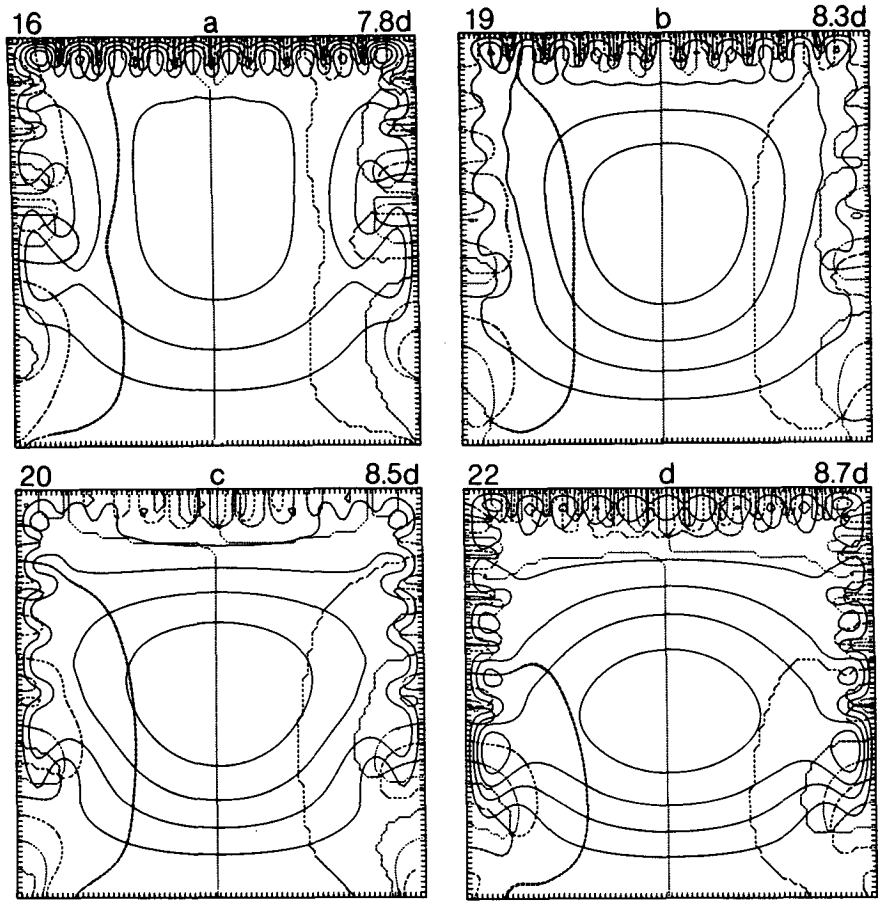

FIG. 8. Volume-transport case with a 3000 m shelf depth. Examples of modes with large-scale interior response resembling the fundamental flat-bottom mode of Fig. 3. Contouring as in Fig. 2. (a) Mode 16, period 7.8 days. (b) Mode 19, period 8.3 days. (c) Mode 20, period 8.5 days. (d) Mode 22, period 8.7 days. Compare with the quasi-geostrophic case of Fig. 5. Notice the effect of the fully varying topography in causing shelf modes with higher modal structure to populate the fundamental β-mode frequency range.

As a summary of the volume-transport cases, we present Fig. 9, a graphical illustration of spectral density and strength of interior response for the volume-transport eigenmodes (flat bottom, 3000, 2000 and 1000 m shelf depths). Normalizing the modes according to the relation

$$\iint_{\text{basin}} \Phi_n J(\Phi_n^*, f/H)dxdy = i, \tag{3.1}$$

we compute a measure of their tide-gauge signal strength in the ocean interior, namely,

$$I \equiv \iint_{\text{interior}} \Phi_n \Phi_n^* dxdy \tag{3.2}$$

where the domain of integration is the 3000 km-square, flat region of the basin. The value of I is then normalized with respect to its value for the fundamental flat-bottom mode and plotted versus mode frequency. (Although geostrophically balanced model sea level fluctuations are not directly proportional to Φ, owing to the spatial variability of f and H, they are approximately so in the flat interior. Thus, we may also interpret I to be roughly proportional to interior-ocean potential energy.)

The fascinating break-up of the flat-bottom modes into families of large-scale planetary/shelf modes is clearly evident in Fig. 9. Individual modes within a family often resemble a flat-bottom counterpart and are labeled accordingly. Those families with no consistently clear resemblance are marked with (?). Oscillations predominantly confined to shelf regions appear in Fig. 9 as short lines. Thus, modes with large I are more likely to be observable at an open-ocean tide gauge. If two or more modes with nearly the same frequency contribute to a tide gauge record, the damped, resonant peaks may overlap, yielding a broadbanded appearance in the resultant frequency spectrum. Therefore, a cautious interpretation of data from tide gauges is particularly important for vorticity modes.

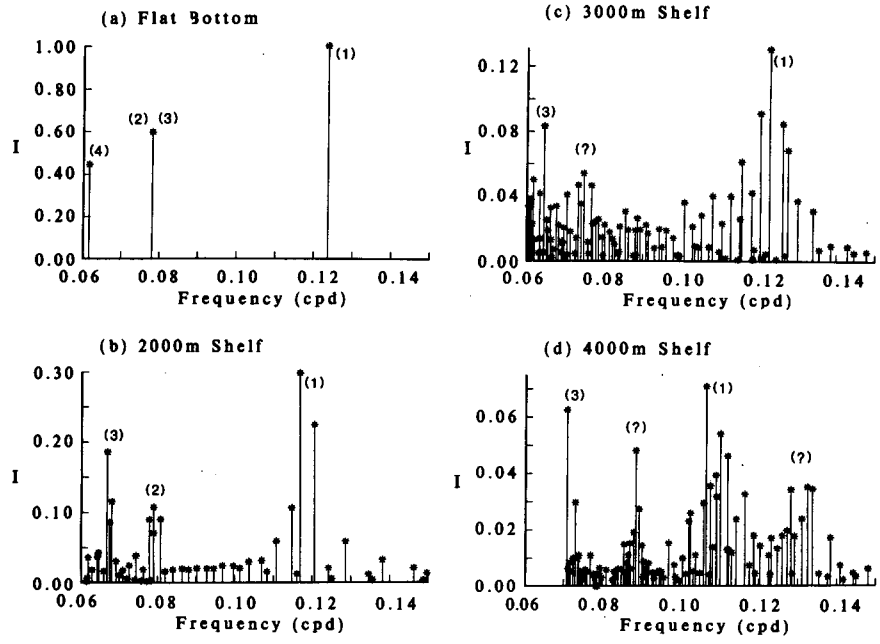

FIG. 9. Volume-transport case with various shelf heights. Graphical depiction of the strength of interior response, I, defined in (3.2) and normalized by the fundamental flat-bottom mode value, versus mode frequency. Large values of I correspond to strong interior response while small values indicate the response is primarily trapped to the shelf regions. (a) Flat bottom case. (b) 3000 m shelf depth. (c) 2000 m shelf depth. (d) 1000 m shelf depth. The emergence of a family of modes with large-scale interior response resembling the nondegenerate flat-bottom mode (1) of (a) is clearly evident in (b), (c) and (d). The degenerate pair, (2) and (3), is split (in the classical, perturbative sense) into two separate families in (b).

Another measure of the open-ocean amplitude of the planetary/shelf modes is the fraction of total variance individually explained by them in an expansion of a β-mode. Thus, we expand a flat-bottom mode, say, Θ_n, in terms of the planetary/shelf modes, Φ_m,

$$\Theta_n(x, y) = \sum_m a_{mn}\Phi_m(x, y), \tag{3.3}$$

and plot versus frequency the percent of total variance absorbed (Miller, 1986, details the procedure). The frequency bandwidth of a "peak" is indicative of how rapidly currents with planetary scales may leak energy onto shelf regions (see section 5).

Figure 10 shows the results of the expansion (3.3) for the fundamental β-mode (Fig. 3). The structures associated with this fundamental β-mode appear dominantly in two modes of the basin with 3000 m shelf depth. When the steeper shelves are included, the true modes contribute smaller percentages to the description, and the spectral width broadens, suggesting more rapid energy leakage onto shelves. The appearance of two broad peaks (cf. Fig. 9d) for the 1000 m shelf depth is surprising. The expansions of the second and third flat-bottom modes (an analytically, but not computationally, degenerate pair) reveal that they are split into two separate families for the case of the 3000 m shelf depth (Figs. 11a, 12a). In the presence of steeper shelves, this separation is less distinct (cf. Fig. 9c, d). Another dual-peaked structure occurs in the second β-mode expansion for the 2000 m shelf-depth case (Fig. 11b). Note that we did not reduce the scale of the flat-bottom modes to allow for a reduction in basin size due to the presence of the shelves.

Frequency response curves, corresponding to (2.7) with specified forcing and dissipation, will exemplify the production, by these shelf topographies, of broad-bandedness in frequency space. Since the result can be anticipated and the model is so idealized, we defer such an analysis to future studies using realistic ocean basins. We instead investigate the nature of these free oscillations in the next section.

4. Coupled oscillator model

We seek a feasible mechanism for the rending of nondegenerate β-modes into families of planetary/shelf modes in the presence of the shelf topography. Standard perturbation theory can yield only single β-modes, each shifted in frequency and modified in structure. We, therefore, propose a model of coupled planetary-wave/shelf-wave oscillations based on the observation that the solutions (Figs. 4–8) exhibit a tendency for interior structure to resemble flat-bottom modes and shelf structure to resemble topographic modes. Coupled os-

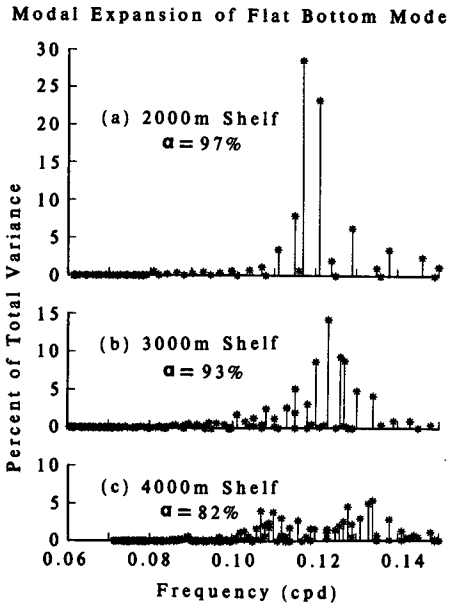

FIG. 10. Volume-transport case with various shelf heights. Percent of total variance absorbed by each volume transport mode coefficient in the expansion (3.3) for the fundamental flat-bottom mode. The expansion reveals the distribution of large-scale structure with frequency. Total variance absorbed by the expansion set is indicated by α. (a) 3000 m shelf depth. (b) 2000 m shelf depth. (c) 1000 m shelf depth. Note that the two broad peaks in (c) are also evident in Fig. 9d.

cillator theory can qualitatively reproduce the phenomenon and provide a simple, intuitive model of the physics.

Restricting ourselves to quasi-geostrophy for this discussion, we seek simplified solutions to (2.4) with

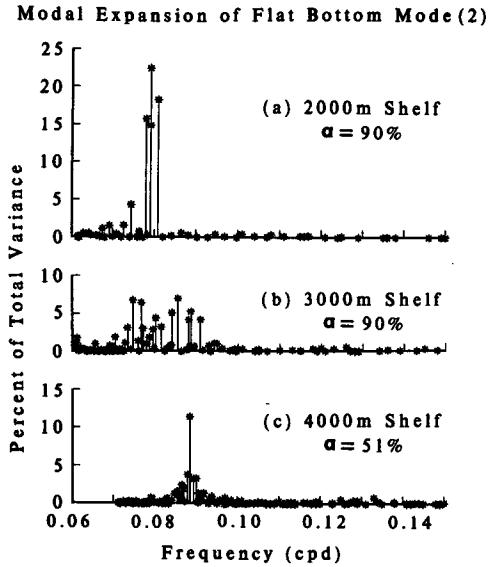

FIG. 11. As in Fig. 10 but for the second flat-bottom mode of original period 12.8 days. The shelf has split the degenerate second and third flat-bottom modes into two separate families (cf. Fig. 9b).

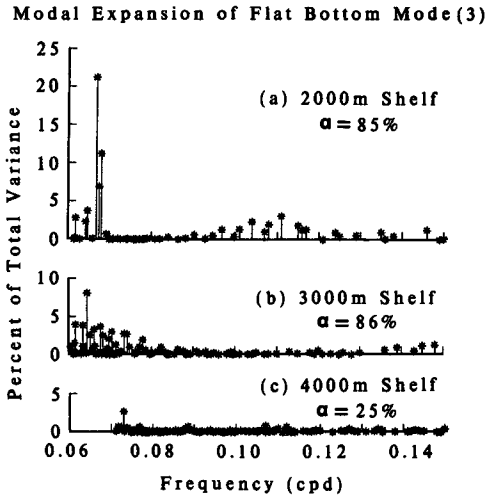

FIG. 12. As in Fig. 11 but for the third flat-bottom mode of original period 12.8 days.

$\phi_n = 0$ on the boundaries. Introduce the sets of solutions (γ_n, P_n) and (ω_n, S_n) such that they satisfy the β-plane, planetary waves case and the f-plane, shelf waves case, respectively, i.e.,

$$i\gamma_n \nabla^2 P_n + \beta \frac{\partial}{\partial x} P_n = 0, \tag{4.1}$$

$$i\omega_n \nabla^2 S_n + \frac{f_0}{H_0} J(S_n, h) = 0. \tag{4.2}$$

Each set forms a complete basis for the expansion of arbitrary functions satisfying the same boundary conditions in the basin.

Let an approximate solution of (2.4) be written as

$$\phi_k = \sum_{n=1}^{N} a_{nk} P_n + \sum_{m=1}^{M} b_{mk} S_m, \tag{4.3}$$

where we include only a few of the highest frequency (or some frequency band of) oscillations of each basis set. (The choice of this basis over any other Galerkin truncation is motivated by the presumably small values of N and M required for convergence.) These basis functions are linearly independent but not orthogonal. Substituting (4.3) into (2.4), multiplying through by the conjugate functions, integrating over the basin, and invoking the orthogonality relations (Rhines and Bretherton, 1973; Miller, 1986)

$$\iint_{\text{basin}} P_n J(P_m^*, \beta y) dx dy = i\delta_{nm}, \tag{4.4}$$

$$\iint_{\text{basin}} S_n J\left(S_m^*, \frac{f_0 h}{H_0}\right) dx dy = i\delta_{nm}, \tag{4.5}$$

results in an $(N + M)$ by $(N + M)$ eigenproblem in the frequency, σ_k (eigenvalue), and the expansion coefficients vector, $(a_n, b_m)_k$ (eigenvector), i.e.,

$$\lambda\left[\left(\frac{\gamma_1}{\gamma_n}\right)a_n-\sum_{m=1}^{M}\left(\frac{i\gamma_1}{\omega_m}\right)\int\int J\left(S_m,\frac{f_0h}{H_0}\right)P_n^*dxdy\right]$$
$$=a_n-\sum_{m=1}^{M}ib_m\int\int J\left(S_m,\beta y+\frac{f_0h}{H_0}\right)P_n^*dxdy-\sum_{l=1}^{N}ia_l\int\int J\left(P_l,\frac{f_0h}{H_0}\right)P_n^*dxdy \quad (4.6a)$$

$$\lambda\left[\left(\frac{\gamma_1}{\omega_m}\right)b_m-\sum_{n=1}^{N}a_n\left(\frac{i\gamma_1}{\gamma_n}\right)\int\int J(P_n,\beta y)S_m^*dxdy\right]$$
$$=b_m-\sum_{n=1}^{N}ia_n\int\int J\left(P_n,\beta y+\frac{f_0h}{H_0}\right)S_m^*dxdy-\sum_{l=1}^{M}ib_l\int\int J(S_l,\beta y)S_m^*dxdy. \quad (4.6b)$$

This may be written schematically as

$$\lambda_k\Gamma\begin{pmatrix}a_n\\b_m\end{pmatrix}_k=\Lambda\begin{pmatrix}a_n\\b_m\end{pmatrix}_k, \quad (4.7)$$

where Γ and Λ are Hermitian matrix operators and $\lambda_k \equiv (\sigma_k/\gamma_1)$. This can be readily solved numerically using standard EISPACK routines.

Not all solutions of (4.6) will be representative solutions of (2.4). True solutions which project strongly on the basis set of (4.3) will have counterparts under the approximation. But since $(N + M)$ eigensolutions will necessarily be present, some approximate solutions will be spurious due to the incomplete expansion basis in (4.3).

As an example, consider the 3000 m shelf depth of section 3b. In this case, the P_n are the flat-bottom, β-plane Rossby modes and the S_n are the f-plane shelf modes of section 3a. Solutions for $N = 6$ (the first six flat-bottom modes) and $M = 24$ (the first six groups of four shelf modes) have many features in common with the full solutions. (Smaller values of N and M result in qualitatively, but less quantitatively, satisfactory solutions.) For instance, the splitting of the fundamental shelf-wave group via the β-plane perturbation is shown in Fig. 13, which may be directly compared to Fig. 4. The eigenfunctions are almost identical. Frequency errors are all less than 4 percent. An example of the generation of a family of β-modes is shown in Fig. 14, which may be directly compared to Fig. 5. The structural similarity between the model solutions and true solutions is remarkable. Errors in frequency are all less than 3 percent. Many of the other model solutions for this case also correspond well to their full solution counterparts. The planetary-wave/shelf-wave coupled oscillator model thus provides a successful interpretation of the full solutions.

5. Discussion

In the presence of an imperfectly reflecting boundary, flat-bottom, β-plane normal modes experience an extension of their influence in frequency space. No longer confined to single frequencies, these modes appear as families (Figs. 5 and 8) whose members have frequencies near the original flat-bottom counterpart. This break-up may be interpreted as coupled, planetary-wave/shelf-wave oscillations.

Intuitively, one expects that (4.2) will apply most strongly over the shelf, with (4.1) holding dominantly in the interior. A simple model of coupling shelf motion to the open ocean is

$$\frac{\partial}{\partial t}\nabla^2P+\beta\frac{\partial}{\partial x}P=-\beta\frac{\partial}{\partial x}S, \quad (5.1)$$

$$\frac{\partial}{\partial t}\nabla^2S+J\left(S,\frac{f_0h}{H_0}\right)=-J\left(P,\frac{f_0h}{H_0}\right), \quad (5.2)$$

where (5.1) holds in the interior and (5.2) holds on the shelf region. The left-hand sides represent the lowest-order balance, while the right-hand sides represent higher-order coupling. In particular, we anticipate the dominant coupling effect to be a β-induced shelf-wave forcing of the interior flow and a topography-induced planetary-wave forcing of motion on the shelf, respectively (cf. Rhines and Bretherton, 1973, pp. 599–600). These equations bear the form of coupled oscillators; the normal modes of such coupled systems are usually approximated as linear combinations of solutions of the decoupled system. This qualitatively explains the repeated β-mode structures in solutions of the full equations, and motivates the expansion in (4.3). [Solutions of (4.6) might be taken as the starting point of an iterative scheme for generating solutions for topographic domains which are computationally unresolvable.]

Much like coupled oscillator phenomena of classical physics (e.g., Sommerfeld, 1952), which can be generalized to multiple degree-of-freedom systems, planetary waves of the interior may exchange energy with shelf waves of similar frequency. The spectral "bandwidth" of a family of planetary/shelf modes provides a measure of the efficiency of energy leakage from the interior to shelf regions. For example, in the case of the 3000 m shelf depth, we may estimate the time scale of destruction (by the shelf topography) of the fundamental, flat-bottom, β-mode as

$$\tau\approx\frac{1}{2}\left(\frac{1}{\delta f}\right)\approx 40 \text{ days}, \quad (5.3)$$

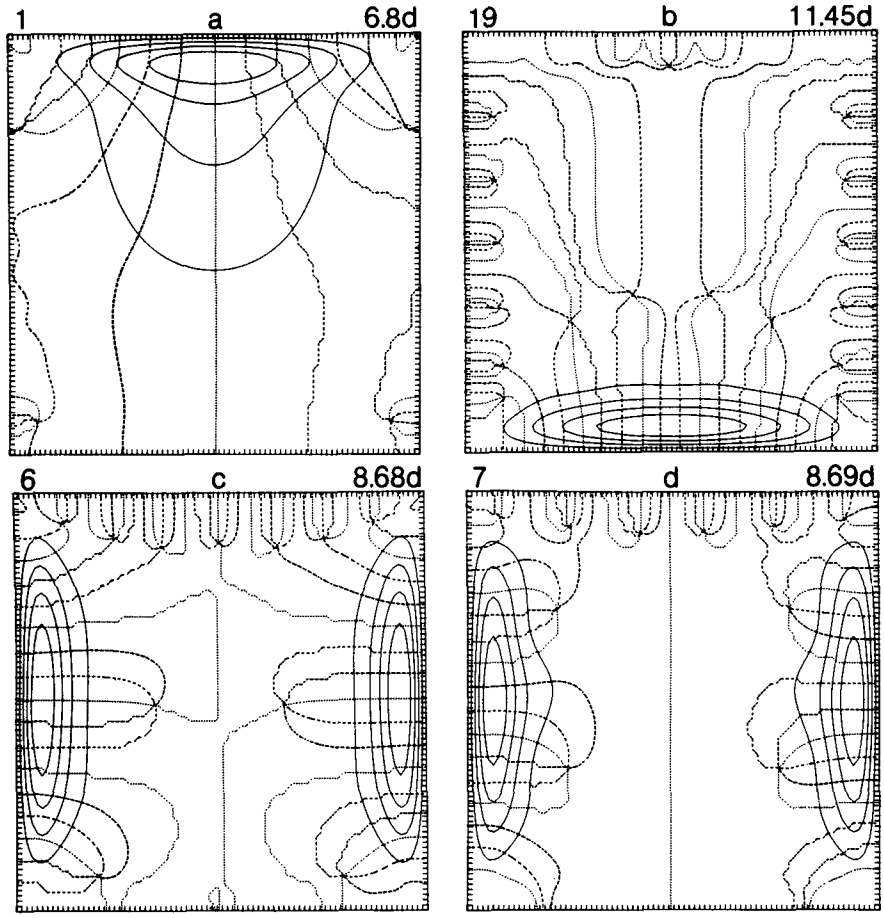

FIG. 13. Quasi-geostrophic β-plane case with a 3000 m shelf. Solutions of the coupled planetary-waves/shelf-waves model (section 4) which may be directly compared to Fig. 4. (a) Mode 1, period 6.8 days. (b) Mode 19, period 11.45 days. (c) Mode 6, period 8.68 days. (c) Mode 7, period 8.69 days.

where $\delta f \approx$ (0.128–0.115) cpd is the frequency bandwidth for modes with similar interior structure (Figs. 8, 10a, 9b). This break-up can be visualized with an initial value problem. We expand the fundamental flat-bottom mode in a sum of planetary/shelf modes, as in (3.3), and allow it to oscillate with natural frequencies. This is shown in Fig. 15 as a time sequence. The initial large-scale pattern leaks energy onto the northwestern shelf region over a 40 day time scale, as anticipated above. The region of the shelf onto which energy leaks is not easily anticipated by inspection of mode structures in Fig. 8.

The resonance curves for a given forcing function will be much more spikey in the model ocean interior when a shelf is present. Moderate dissipation will broaden the spikes, causing the peaks associated with a family of modes (e.g., Fig. 9b–d) to overlap, forming a broadbanded peak. This will be particularly noticeable for a family that is relatively isolated in frequency from other families. The oceanographically relevant point is that a family of modes excited at resonance may appear as a broadband peak in sea level spectra, particularly when the peak is obscured by ambient noise or is poorly resolved due to record length limitations. If a frictional damping parameter is then estimated under the assumption that a single flat-bottom mode is present, it will be overestimated. Although the results of this idealized model cannot be directly applied to Pacific Ocean tide gauge observations of vorticity mode signals (Luther, 1980; 1982), such an analysis will be possible after Pacific basin geometry and free-surface effects are incorporated.

Realistically, other effects may alter the scenario revealed by the models of section 2. The most obvious weakness is our inability to employ a realistically narrow shelf, O(10–100 km), owing to limited resolution. Presumably, the shelf oscillations are much more weakly coupled to interior planetary modes in that situation, although the solutions of section 3c indicate that a steeper shelf produces a stronger interaction than a less steep one. Nevertheless, in companion computations of normal modes with a midocean ridge (and

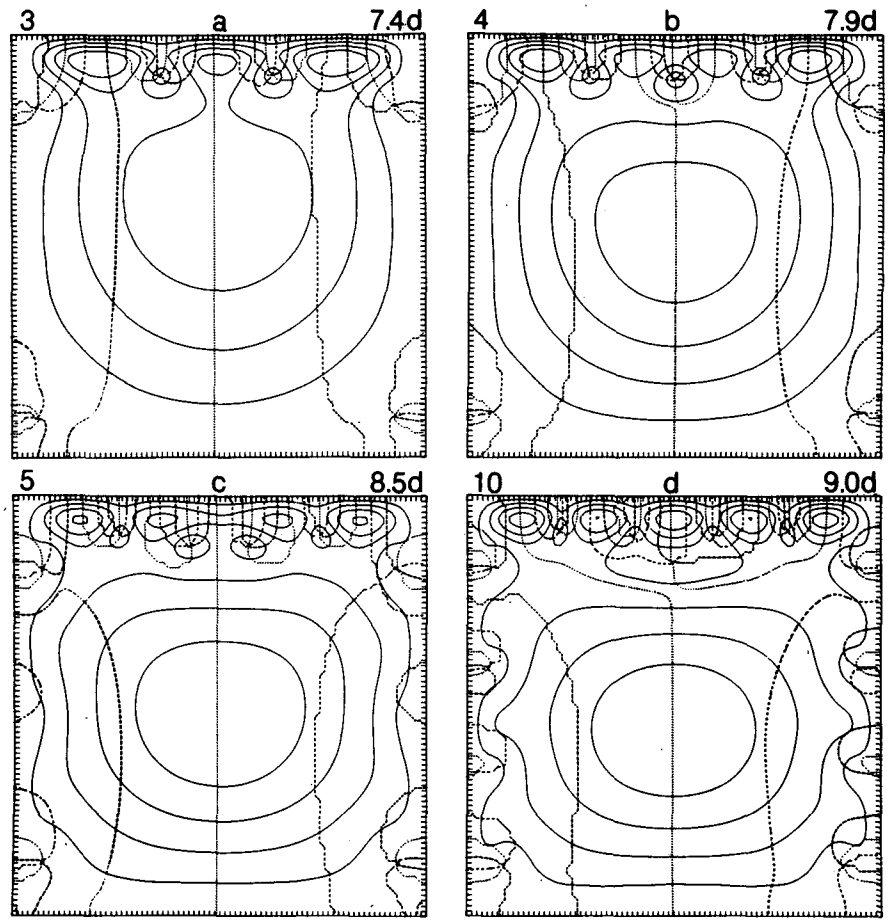

FIG. 14. As in Fig. 13 but for modes with interior response resembling the fundamental flat-bottom modes. Compare to Fig. 5. (a) Mode 3, period 7.4 days. (b) Mode 4, period 7.9 days. (c) Mode 5, period 8.5 days. (d) Mode 10, period 9.0 days. Notice the remarkable degree of similarity of shelf region response and interior structure between the true and approximate solutions.

no shelf), a similar situation occurs. We find that families of β-like sub-basin modes (Rhines, 1969; Anderson and Killworth, 1977) occur on either side of the ridge. Other generic types of topography (rough bottoms, isolated seamounts), however, often only weakly perturb the large-scale, planetary-mode spectrum; the coupling between planetary motion and these types of topographic waves is evidently weak (Miller, 1986).

Further complications arise when considering the possible effects of stratification. The turning latitudes observed in the solutions of section 3c may instead be places where scattering into or from internal Kelvin waves occurs (Allen and Romea, 1980; Suginohara, 1981). Also, equatorial regions are a waveguide for baroclinic waves with frequencies and phase propagation similar to barotropic planetary modes. Coupling of internal to external flows via topography (e.g., Rhines, 1970) or Coriolis effects (Miles, 1974) may be more than a weak perturbation to basin-scale waves. Further studies of these effects are needed to fully interpret Luther's (1980; 1982) observations.

6. Conclusion

Models of low-frequency response in ocean basins typically represent boundary regions as a vertical wall. We have shown that the presence of a continental shelf causes the linear response in the flat interior, far removed from the boundary region, to be very different than that for a completely flat-bottomed ocean. The spectrum of eigenmodes having strong interior response becomes more dense. There arise eigenmode families, each with interior structure corresponding to a flat-bottom β-mode, grouped in frequency bands near the flat-bottom counterpart frequency. We interpret this to be a strong resonance between shelf oscillations and planetary modes. Our proposed mechanism of coupled, planetary-wave/shelf-wave oscillations explains how interior response can resemble flat-bottom modes at multiple frequencies. Since the original flat-bottom mode is nondegenerate, the appearance of a family of modes is distinct from the splitting of multiplets (degenerate eigenmodes) into sets of singlets (perturbed

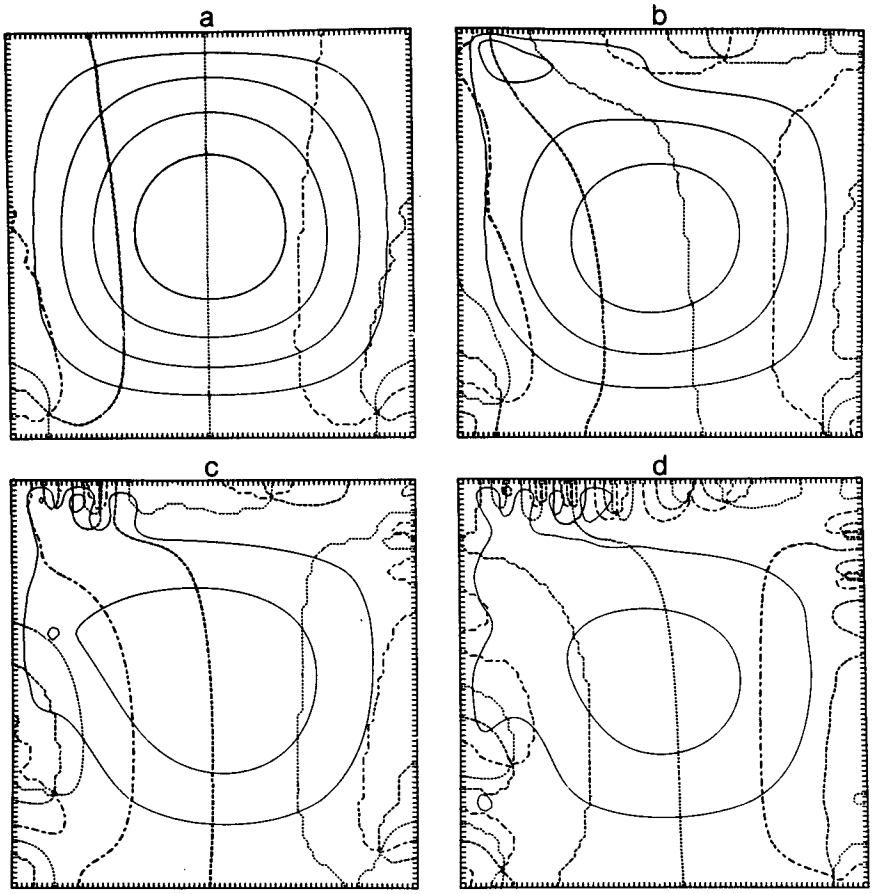

FIG. 15. Time sequence of modal representation of the fundamental flat-bottom mode for the 3000 m shelf-depth volume-transport basis as in (3.3). Ninety-seven percent of the variance of the flat-bottom mode is absorbed by this expansion which includes 61 modes, not many of which had significant amplitude (cf. Fig. 10a). Contour intervals of streamfunction amplitude are constant from plot to plot. (a) Time = 0, Amplitude = 1.00. (b) T = 8 days, Amp = 0.79. (c) T = 24 days, Amp = 0.60. (d) T = 36 days, Amp = 0.52. The interior portion of the flow oscillates primarily at the four frequencies corresponding to the modes of Fig. 8. Energy leaks relatively rapidly onto the northwest shelf region. In the case of the 2000 m shelf depth the leakage occurs on the southwest shelf region.

nondegenerate eigenmodes) by weak perturbations. The present situation involves a strong perturbation of the spectrum of solutions.

Attempts to observe basinwide vorticity modes may be confounded by this topographic effect. Presumably, moderate dissipation would render a band of resonantly excited modes into a "broadband" power spectral structure near the frequency predicted by flat-bottom theory for a single mode. Estimates of dissipation and $(1/Q)$ from an improperly interpreted broadband peak might therefore be unrealistically large.

Acknowledgments. It is a pleasure to acknowledge my interaction with Myrl Hendershott and Doug Luther, who drew my attention to the fascinating questions regarding oceanic vorticity modes. I greatly appreciate George Platzman's generosity both in providing considerable advice and in supplying his world ocean eigencode, which indeed made this study practicable. I thank Mark Swenson, John Miles, Rick Salmon, Bob Hall, Don Altman, Chris Garrett and James Bunch for many useful conversations and criticisms. The National Science Foundation provided financial support under grants OCE81-08703 and OCE84-10067 and computer resources through the National Center for Atmospheric Resarch. This study formed a part of my Ph.D. dissertation at the Institute of Geophysics and Planetary Physics of the Scripps Institution of Oceanography.

REFERENCES

Allen, J. S., and R. D. Romea, 1980: On coastal trapped waves at low latitudes in a stratified ocean. *J. Fluid Mech.*, **98,** 555–585.

Anderson, D. L. T., and P. D. Killworth, 1977: Spin-up of a stratified ocean, with topography. *Deep Sea Res.*, **24,** 709–732.

Arakawa, A., 1966: Computational design for long term numerical integration of the equations of fluid motion. Part I. *J. Comput. Phys.*, **1**, 119–143.

Christensen, Jr., N., 1973: The effect of a coastal shelf on long waves in a rotating hemispherical basin. *J. Mar. Res.*, **31**, 175–187.

Dahlen, F. A., 1968: The normal modes of a rotating, elliptical Earth. *Geophys. J. Roy. Astron. Soc.*, **16**, 329–367.

Flierl, G. R., 1977: Simple applications of McWilliams' "A note on a quasigeostrophic model in a multiply connected domain." *Dyn. Atmos. Oceans*, **1**, 443–453.

Gill, A. E., 1982: *Atmosphere-Ocean Dynamics*, Academic Pres, 662 pp.

Lamb, H., 1932: *Hydrodynamics*, 6th ed., Dover, 738 pp.

Longuet-Higgins, M. S., and G. S. Pond, 1970: The free oscillations of fluid on a hemisphere bounded by meridians of longitude. *Phil. Trans. Roy. Soc. London, A*, **266**, 193–233.

Luther, D. S., 1980: Observations of long period waves in the tropical ocean and atmosphere. Ph.D. dissertation, Joint Program in Oceanography, Massachusetts Institute of Technology and the Woods Hole Oceanographic Institution, 210 pp.

——, 1982: Evidence of a four to six day, barotropic, planetary oscillation of the Pacific Ocean. *J. Phys. Oceanogr.*, **12**, 644–657.

——, 1983: Why haven't you seen an ocean mode lately? *Ocean Modelling*, **50**, 1–6.

Miles, J. W., 1974: On Laplace's tidal equations. *J. Fluid Mech.*, **66**, 241–260.

Miller, A. J., 1986: Barotropic planetary–topographic oscillations in ocean basins. Ph.D. dissertation, Scripps Institution of Oceanography, University of California, San Diego, 133 pp.

Pedlosky, J., 1979: *Geophysical Fluid Dynamics*, Springer-Verlag, 624 pp.

Platzman, G. W., 1978: Normal modes of the world ocean. Part I. Design of a finite element barotropic model. *J. Phys. Oceanogr.*, **8**, 323–343.

——, 1981a: A guide to FORTRAN programs for normal modes of the ocean. Vol. I. The University of Chicago. Tech. Rep. to the National Science Foundation, 81 pp.

——, 1985: Normal modes of the world ocean: Maps and tables. The University of Chicago. Tech. Rep. to the National Science Foundation, 97 pp.

——, G. A. Curtis, K. S. Hansen and R. D. Slater, 1981b: Normal modes of the world ocean. Part II. Description of modes in the period range 8 to 80 hours. *J. Phys. Oceanogr.*, **11**, 579–603.

Rhines, P. B., 1969: Slow oscillations in an ocean of varying depth. Part I. Abrupt topography. *J. Fluid Mech.*, **37**, 161–189.

——, 1970: Edge-, bottom-, and Rossby waves in a rotating, stratified ocean. *Geophys. Fluid Dyn.*, **1**, 273–302.

——, and F. P. Bretherton, 1973: Topographic Rossby waves in a rough-bottomed ocean. *J. Fluid. Mech.*, **61**, 583–607.

Sommerfeld, A., 1952: *Mechanics. Lectures on Theoretical Physics. Vol. I*, Academic Press, 289 pp.

Suginohara, N., 1981: Propagation of coastal-trapped waves at low latitudes in a stratified ocean with continental shelf slope. *J. Phys. Oceanogr.*, **11**, 1113–1122.